Biophysical Journal, Volume *119*

Supplemental Information

Pulsed Electric Fields Can Create Pores in the Voltage Sensors of Voltage-Gated Ion Channels

Lea Rems, Marina A. Kasimova, Ilaria Testa, and Lucie Delemotte

S1. Movie captions

Movie S1: Side view of the formation of a complex pore in VSD4 of NavMs at hyperpolarizing TMV. Snapshots were taken from the entire trajectory (0-200 ns). The VSDs are represented as red ribbons, the rest of the protein is represented as cyan ribbons. Water molecules are represented as transparent volume, whereas phosphorus atoms of lipid headgroups, Na+ ions, and Cl- ions, are shown as gold, yellow, and green spheres, respectively.

Movie S2: Same as in Movie S1, but viewed from the extracellular medium. Water and ions are omitted from representation.

Movie S3: Side view of the formation of a complex pore in VSD2 of NavPaS at hyperpolarizing TMV. Snapshots were taken between 200 ns and 370 ns of the trajectory. Representation of atoms is as in Movie S1.

Movie S4: Same as in Movie S3, but viewed from the extracellular medium. Water and ions are omitted from representation.

Movie S5: Side view of the formation of a lipid pore in HCN1 at hyperpolarizing TMV. Snapshots were taken between 100 ns and 230 ns of the trajectory. Representation of atoms is as in Movie S1.

Movie S6: Same as in Movie S5, but viewed from the extracellular medium. Water and ions are omitted from representation.

Movie S7: Salt bridges reorganization in VSD2 of NavMs at hyperpolarizing TMV. The first and second half of the movie correspond to, respectively, 200 ns during and 200 ns after electric field application. Positively charged ARG, HIS, and LYS are colored green, negatively charged residues ASP and GLU are colored magenta.

S2. Composition of MD systems

Table S1: List of molecules in each MD system

	NavMs	**NavPaS**	**HCN**
Number of lipids	362 POPC	350 POPC	342 POPC
Number of water mol.	48004 TIP3P	54538 TIP3P	50779 TIP3P
Number of ions	133 SOD, 145 CLA	167 SOD, 152 CLA	151 SOD, 151 CLA
Box size (nm)	12.1 x 12.0 x 13.8	12.0 x 11.9 x 15.4	12.2 x 12.1 x 14.9
Total number of atoms	209838	230928	230815
Ion concentration (bulk)	~170 mM	~160 mM	~170 mM

S3. Additional information for electric field simulations

Table S2 reports additional information for the simulations presented in Figure 2 of the main manuscript. The table lists the type of pores that formed in a given simulation (channel pore, VSD pore, complex pore), the time after the onset of an electric field at which the first Na^+ or Cl^- passed a given pore, and the total number of ions that passed a given pore by the end of the simulation. The table also estimates the pore conductance G_{ion} as the ratio of the average electric current I_{ion} that passed through the pore and the transmembrane voltage (TMV = 1.5V) according to equation

$$G_{ion} = \frac{I_{ion}}{TMV} = \frac{q_e N_{ion}}{t_{sim} - t_{ion}} \frac{1}{TMV} \quad \text{(S1)}$$

where q_e, N_{ion}, t_{sim}, and t_{ion} are, respectively, the elementary charge, total number of ions that passed the pore, simulation time and the time of the first ion passage. The last column shows the time at which the second lipid phosphorus atom close to VSD pore was found within 0.5 nm from the center of the lipid bilayer.

Table S2: Analysis of simulations carried out for different channels under TMV of ±1.5 V.

Channel	Simulation name	Ez (V/nm)	zbox (nm)	Sim. length t_{sim} (ns)	Pore type*	Time of first ion passage t_{ion} (ns)		No. passed ions N_{ion}		Conductance G_{ion} (pS)		Time lipids (ns)
						Na	Cl	Na	Cl	G_{Na}	G_{Cl}	
NavMs	[hyp 1.5V #1]	-0.1087	13.8	200	channel	48	-	25	-	18	-	-
					VSD4*	132	89	332	728	524	703	165
					VSD1	-	119	0	1	-	1	-
	[hyp 1.5V #2]	-0.1087	13.8	215	channel	17	-	5	-	3	-	-
					VSD3*	141	112	188	512	270	528	177
					VSD4*	183	176	15	85	50	235	192
	[dep 1.5V #1]	0.1087	13.8	400	channel	42	-	55	-	16	-	-
					VSD2	104	-	3	0	1	-	-
					VSD4	263	246	7	6	5	4	-
	[dep 1.5V #2]	0.1087	13.8	400	channel	41	-	52	-	15	-	-
					VSD2	145	155	1	1	0	0	-
NavPaS	[hyp 1.5V #2]	-0.0973	15.4	200	VSD2*	120	124	101	167	135	236	189
	[hyp 1.5V #1]	-0.0973	15.4	345	VSD1	233	165	1	9	1	6	-
					VSD2*	249	268	64	109	80	175	334
	[dep 1.5V #1]	0.0973	15.4	200	lipid	191	190	46	87	517	924	188
					VSD1	90	80	8	7	8	6	-
	[dep 1.5V #2]	0.0973	15.4	377	VSD2*	350	344	61	123	239	391	370
					VSD1	364	-	1	0	8	-	-
HCN1 wt	[hyp 1.5V #1]	-0.1007	14.9	230	lipid	207	207	239	505	1105	2373	208
	[hyp 1.5V #2]	-0.1007	14.9	546	lipid	510	510	436	849	1300	2535	512
					VSD4	497	-	2	0	4	-	-
	[dep 1.5V]	0.1007	14.9	600	-	-	-	-	-	-	-	-
HCN1 mut	[hyp 1.5V #1]	-0.0992	15.1	430	VSD3*	248	313	469	848	201	494	383
					VSD4	356	398	26	51	20	55	-
	[hyp 1.5V #2]	-0.0992	15.1	432	lipid	395	393	362	821	963	2086	397

* VSD pore expanded into a complex pore.

Here we present additional results from simulations. For each simulation we determined the number of ions that passed through a given pore, the number of lipids that stabilized a given pore, and the minimum radius of all VSDs and the channel pore. Furthermore, we divided each channel into 7 different parts: VSD1, VSD2, VSD3, VSD4, all S5 segments, all pore helices, and all S6 segments, as indicated in Table S3. For each of these parts of the protein we determined the change in the number of residues in helical structure and the change in the solvent accessible surface area. The results are presented in Figs. S1-S4. Below we show an example, which helps explain how to read the graphs.

Table S3: List of residues, which were assigned to different parts of the channel: VSD1, VSD2, VSD3, VSD4, S5 segments, pore helices (PH) and S6 segments.

	NavMs	NavPaS	HCN1
VSD1	-1:113 (subdomain 1)	140:241	140:290 (subdomain 1)
VSD2	-1:113 (subdomain 2)	519:624	140:290 (subdomain 2)
VSD3	-1:113 (subdomain 3)	856:965	140:290 (subdomain 3)
VSD4	-1:113 (subdomain 4)	1171:1277	140:290 (subdomain 4)
all S5	114:155 (all subdomains)	242:280, 625:670, 966:1004, 1278:1321	291:326 (all subdomains)
all PH	163:193 (all subdomains)	361:389, 687:714, 1048:1073, 1339:1363	327:368 (all subdomains)
all S6	194:235 (all subdomains)	390:425, 715:746, 1087:1124, 1384:1424	369:401(all subdomains)

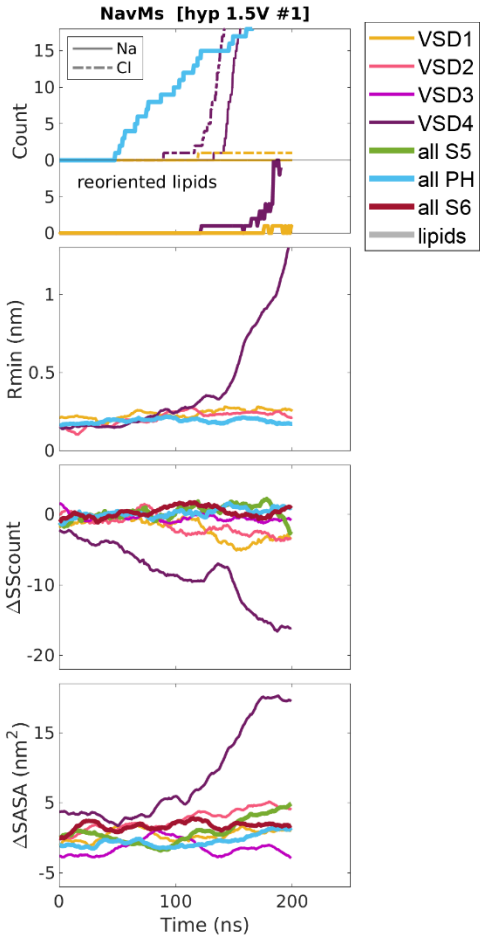

Different line colors code for different parts of the protein, as shown in the legend. The x axis (time) is limited to a 250-ns long region of interest.

The upper part of the first (top) graph shows the progression of the cumulative sum of the number of Na and Cl ions that passed a given pore (channel pore, VSD pore/complex pore, or lipid pore). The lower part of the first graph shows the number of lipids that were found within 0.5 nm of the membrane center and stabilized a given pore.

The second graph shows the radius of the central channel pore and the radius of the pathway along each VSD (this pathway can expand into a VSD pore/complex pore). The radius was determined as the radius of the biggest sphere that can be pushed through the entire pathway.

The third and fourth graph, respectively, show the change in the number of residues that are in helical structure (α-helix, π-helix, 3_{10} helix) and the change in the solvent accessible surface area (SASA), for each part of the channel. The change is calculated vs. the average value from a 200-ns long trajectory under zero electric field.

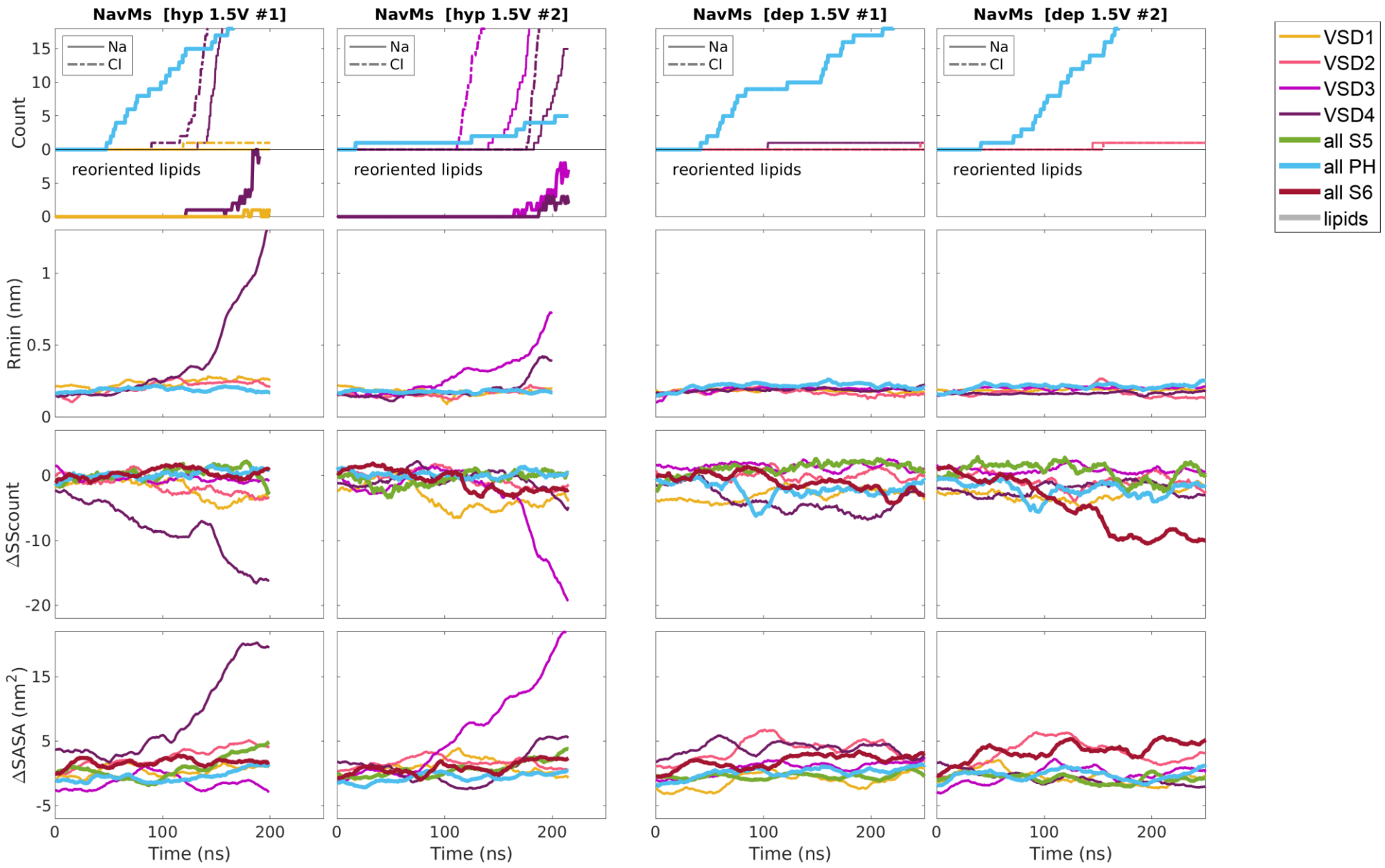

Fig. S1: Additional results for simulations of NavMs under applied electric field. See above for a detailed explanation on how to read the graphs.

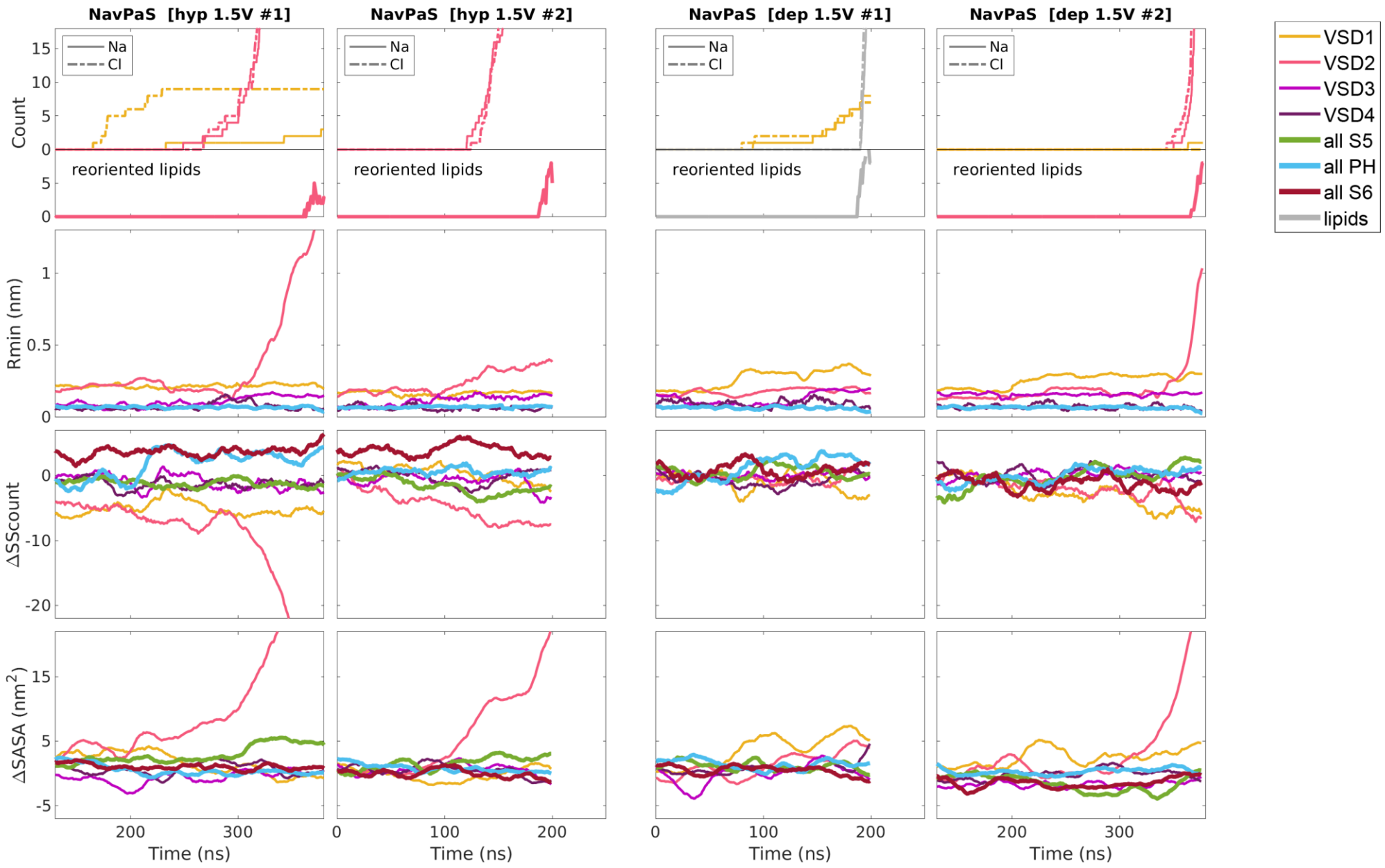

Fig. S2: Additional results for simulations of NavPaS under applied electric field. See above for a detailed explanation on how to read the graphs.

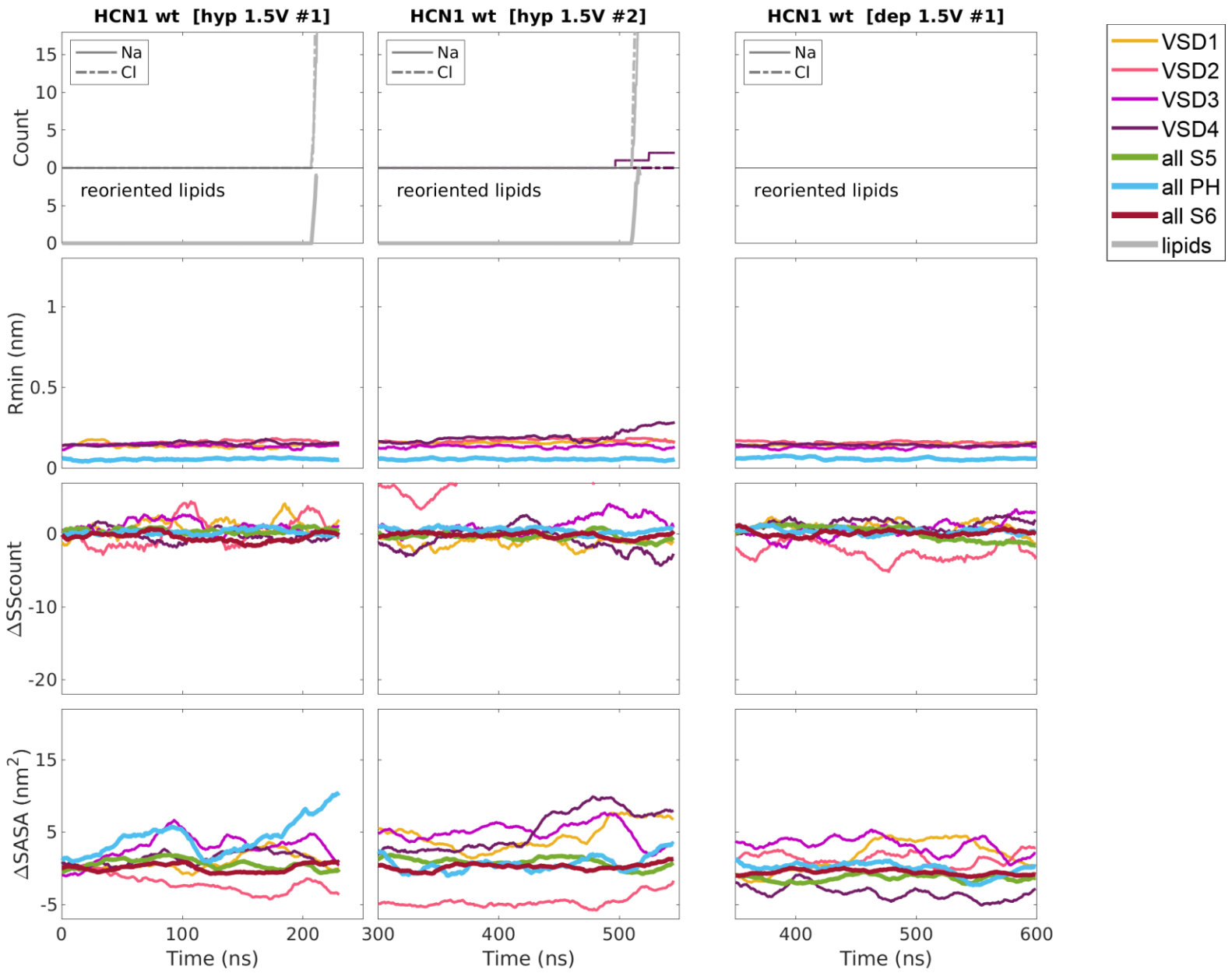

Fig. S3: Additional results for simulations of HCN1 wild type under applied electric field. See above for a detailed explanation on how to read the graphs.

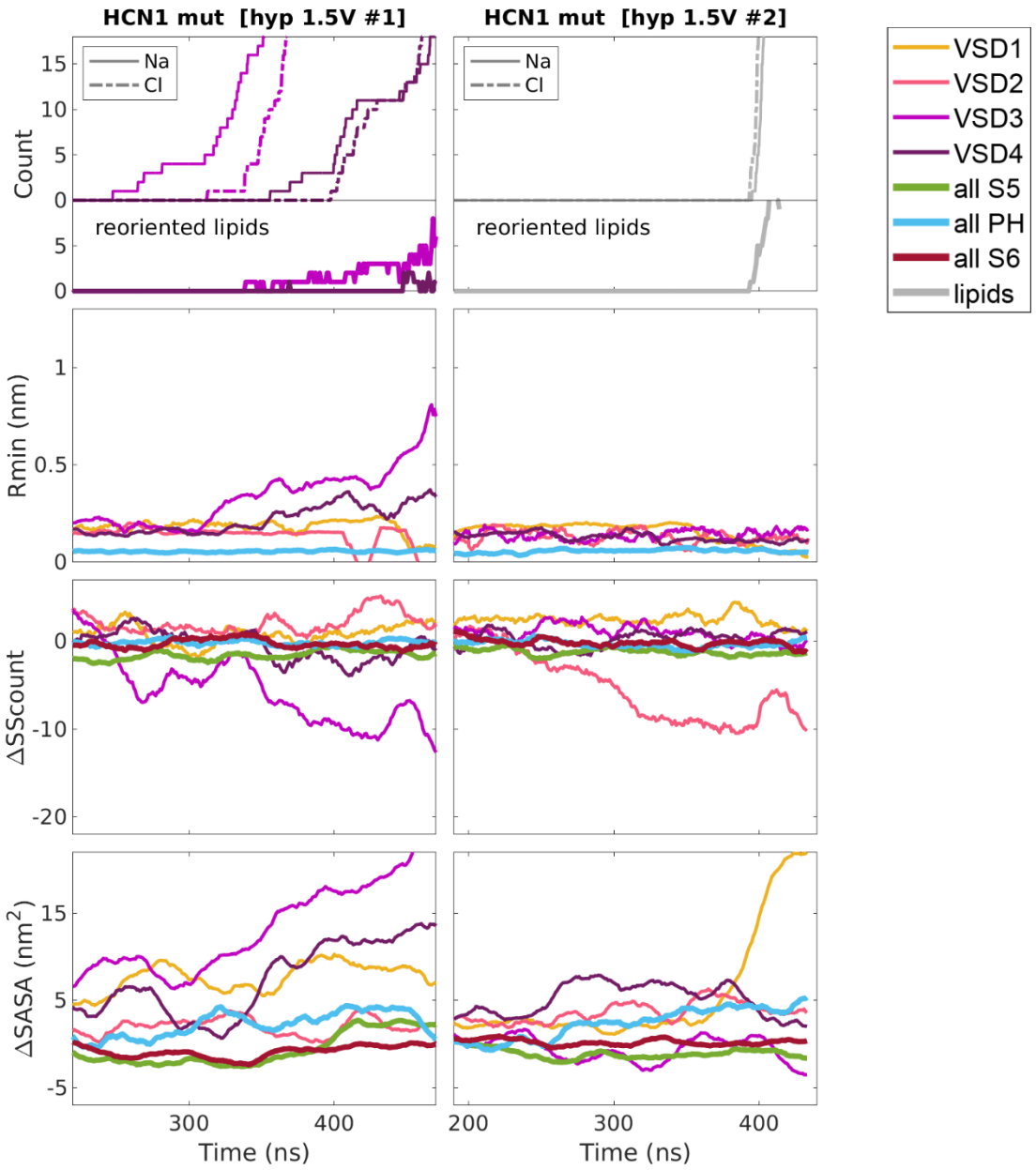

Fig. S4: Additional results for simulations of HCN1 mutant under applied electric field. See above for a detailed explanation on how to read the graphs.

S4. Control simulations

The results presented in the manuscript were obtained by applying a constant electric field and maintaining the NVT ensemble, which kept the simulation box size constant. To test how results depend on the simulation method, we performed additional control simulations for the NavMs channel by applying constant electric field by in NPT ensemble and by applying a constant charge imbalance across the membrane.

S4.1 NPT simulations

NPT simulations were performed in the same way as NVT simulations, except that we controlled the pressure using the Parrinello-Rahman barostat (τ = 5 ps, P = 1 bar, semi-isotropic coupling). Two NPT simulations were performed under hyperpolarizing field and two under depolarizing field. In NPT simulations we observed similar events as in NVT simulations. First, Na^+ ions started passing through central channel pore. Then, one or more VSD pores formed. VSD pores expanded into complex pores under hyperpolarizing TMV. In the first simulation under hyperpolarizing field a VSD pore initiated in VSD3, transformed into a complex pore. This complex pore did not continue to expand by unfolding the VSD, it rather expanded into the bilayer (Fig. S6a), similarly as shown for a NavPaS complex pore in Fig. 5b of the main manuscript. However, in the second simulation under hyperpolarizing field, a complex pore formed in VSD2, which continuously expanded by simultaneously unfolding the VSD (Fig. S6b). As expected, no complex pores were observed in either simulation under depolarizing field. Poration of VSDs occurred on similar time scales as in NVT simulations, as can be seen by comparing results from Table S2 and Table S4 or results from Fig. S1 and Fig. S8. Overall, we did not see appreciable differences between NVT and NPT simulations that would affect the results and conclusions presented in the paper. The main difference that can be seen between NPT and NVT simulations is that considerable expansion of complex pores or lipid pores (beyond a diameter of ~3 nm) in NPT simulations leads to continuous expansion of the system in x and y direction until complete destruction of the system, whereas in NVT ensemble the bilayer begins to bend because it cannot expand in x and y direction. In either case the simulations at this point become unrealistic, therefore we omitted these unrealistic parts of the simulations from analysis and interpretation.

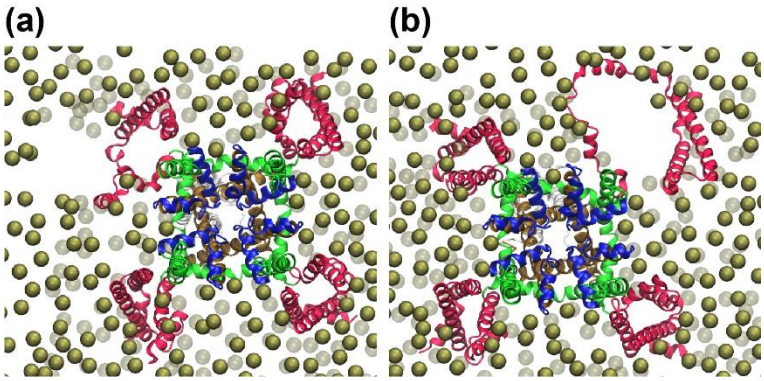

Fig. S6: Extracellular view of the complex pores formed in the first (a) and second (b) NPT simulation under hyperpolarizing field. In the first simulation the pore initiated within one of the VSDs, but then expanded into the bilayer without further unfolding the VSD. In the second simulation, expansion of the complex pore simultaneously continued to unfold the VSD.

Table S4 reports additional information for NPT simulations, similarly as Table S2. Fig. S8 shows additional results in the same way as Figs. S1-S4 (please see section S3 for details on how the data was analyzed).

Table S4: Analysis of control NPT simulations carried out for NavMs channel.

Chan-nel	Simulation name	Ez (V/nm)	zbox (nm)	Sim. length t_{sim} (ns)	Pore type*	Time of first ion passage t_{ion} (ns)		No. passed ions N_{ion}		Conductance G_{ion} (pS)		Time lipids (ns)
						Na	Cl	Na	Cl	G_{Na}	G_{Cl}	
NavMs	[hyp 1.5V NPT #1]	-0.1087	~13.8 NPT	313	channel	24	-	16	-	6	-	-
					VSD3*	152	90	79	302	59	157	287
					VSD2	-	292	0	18	-	614	-
	[hyp 1.5V NPT #2]	-0.1087	~13.8 NPT	174	channel	28	-	8	-	6	-	-
					VSD2*	100	84	162	435	234	518	137
	[dep 1.5V NPT #1]	0.1087	~13.8 NPT	200	channel	166	-	5	-	16	-	-
						-	-	-	-	-	-	-
	[dep 1.5V NPT #2]	0.1087	~13.8 NPT	200	channel	70	-	26	-	21	-	-
					VSD1	168	-	1	-	3	-	-

* VSD pore expanded into a complex pore along the run.

4.2 Charge imbalance

In charge imbalance simulations we separated the water bath by vacuum layer, as shown in Fig. S6. In the first set of simulations we first added ~2 nm thick layer of water and ions, such that upon separating the water baths with vacuum the upper and lower water baths have approximately equal volume (Fig. S7a). For this system we performed one simulation under hyperpolarizing and one simulation under depolarizing TMV. We also prepared a system, where we only separated the water bath by vacuum without adding more water. The upper and lower water baths in this system had different volumes (Fig. S7b). For this system we performed one simulation under hyperpolarizing TMV. In both systems the TMV was built by maintaining a difference in the number of Na and Cl ions in the upper and lower bath using GROMACS' "computational electrophysiology" algorithm. Overall, the difference between the charge within the upper and lower water baths was $34q_e$, where q_e is the elementary charge. Overall, we observed no major differences between simulations with the first and second system. Only the simulations with the first system are reported in the main manuscript.

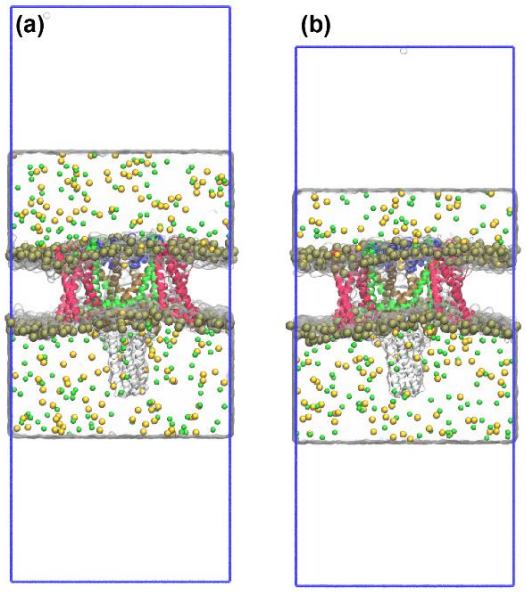

Figure S7: Addition of vacuum in charge imbalance simulations. The blue rectangles show the simulation box size. (a) System with added water molecules, so that the upper and lower water baths have approximately equal volume. (b) System without added water molecules – the upper and lower water baths have different volume.

The differences observed between electric field simulations and charge imbalance simulations are explained in subsection *"Comparison with the charge imbalance method"* of the main manuscript. Briefly, the main difference between electric field and charge imbalance simulations is that in charge imbalance the TMV is affected by formation of pores and continuously drops throughout the simulations. The complex pores formed under hyperpolarizing TMV thus do not expand indefinitely, but their size becomes stabilized. Moreover, the central channel pore stops conducting Na ions after TMV drops sufficiently low. Similarly as in electric field simulations, no complex pores were observed under depolarizing TMV, only a VSD pore formed. Additional results are reported in Table S5 and Fig. S9 (please see section S3 for details on how the data was analyzed).

Table S5: Analysis of charge imbalance simulations carried out for NavMs channel.

Channel	Simulation name	Ez (V/nm)	zbox (nm)	Sim. length t_{sim} (ns)	Pore type*	Time of first ion passage t_{ion} (ns)		No. passed ions N_{ion}		Conductance G_{ion} (pS)		Time lipids (ns)
						Na	Cl	Na	Cl	G_{Na}	G_{Cl}	
NavMs	[hyp CHIMB #1]	ch.imb.	32	200	channel	2	-	3	-	2	-	-
		34qe			VSD1*	33	29	262	947	167	592	50
	[hyp CHIMB #2]	ch.imb.	30	200	channel	12	-	7	-	4	-	-
		34qe			VSD2*	23	18	64	469	39	275	106
					VSD1	36	-	2	-	1	-	-
	[dep CHIMB #1]	ch.imb.	32	170	channel	42	-	14	-	12	-	-
		34qe			VSD3	108	104	1	2	2	3	-

* VSD pore expanded into a complex pore along the run.

4.3 Ionic transport through the central channel pore

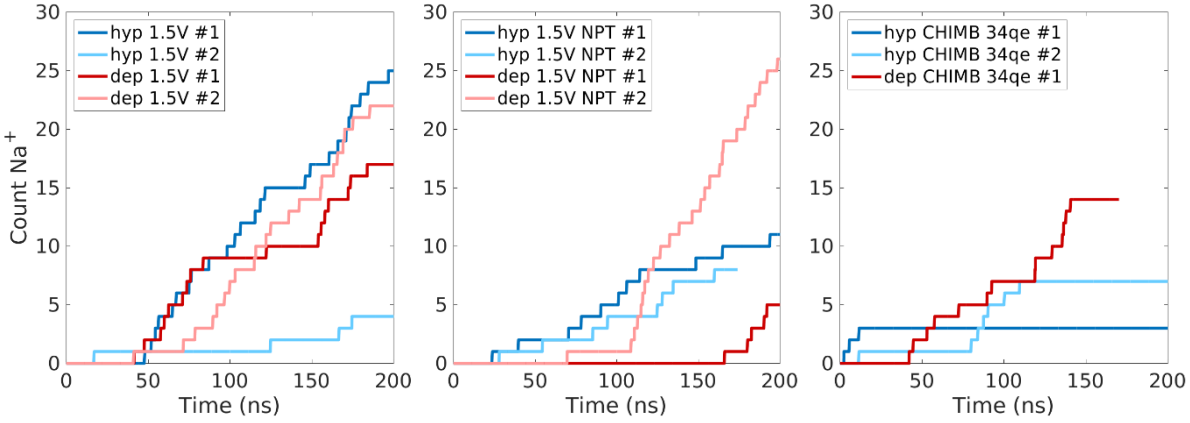

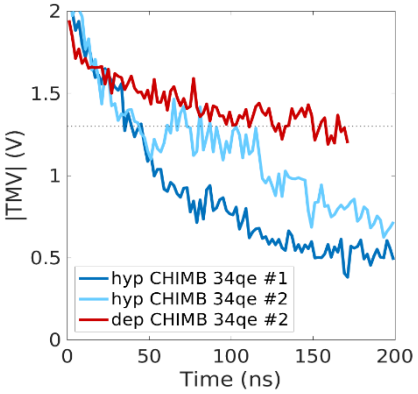

Figure S8: Cumulative sum of Na ions through the central channel pore in NavMs. From left to right: NVT simulations presented in the main manuscript, control NPT simulations, and charge imbalance simulations. The slopes of the curves vary similarly in NVT and NPT simulations. This suggests that the differences between all curves are within the statistical variability on such short simulation time scale. Note that in charge imbalance the central channel pore eventually stops conducting due to decreasing |TMV|.

4.4 Secondary structure perturbation of VSDs with complex pores

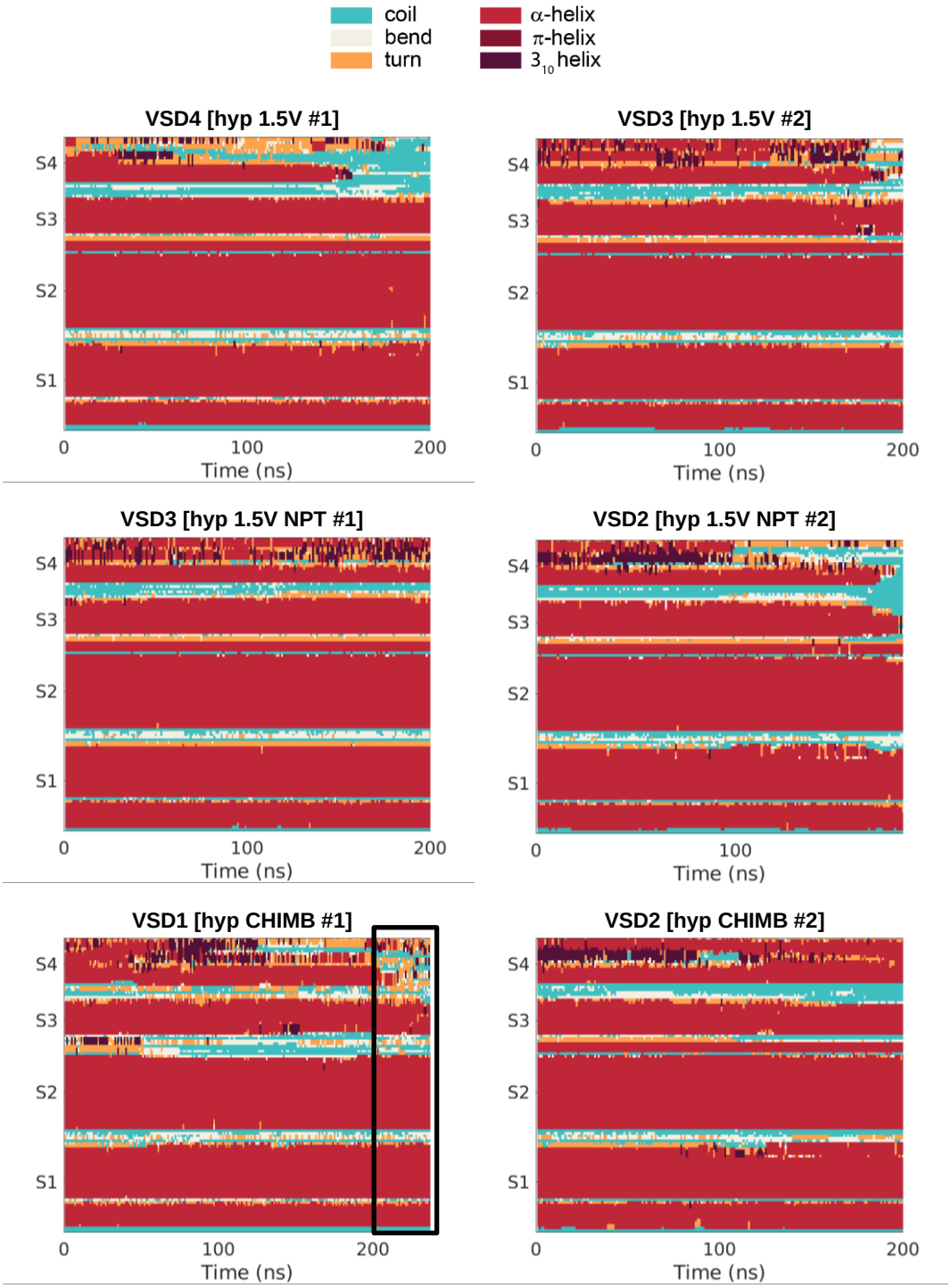

Figure S9: Perturbation of the secondary structure of VSDs with complex pores in NavMs. The structure of S4 is most perturbed. In simulation [hyp 1.5V NPT #1] the VSD is hardly perturbed because the pore expanded out of the VSD into the bilayer, as shown in S6a. In simulation [hyp 1.5V NPT #2] similar unfolding of the VSD is observed as in the main NVT simulations shown in the first row. In simulation [hyp CHIMB #1] the part in the black rectangle shows the simulation where the charge imbalance was increased to $44q_e$ upon formation of a complex pore. The unfolding of VSD in this part is comparable to the main NVT simulations shown in the first row.

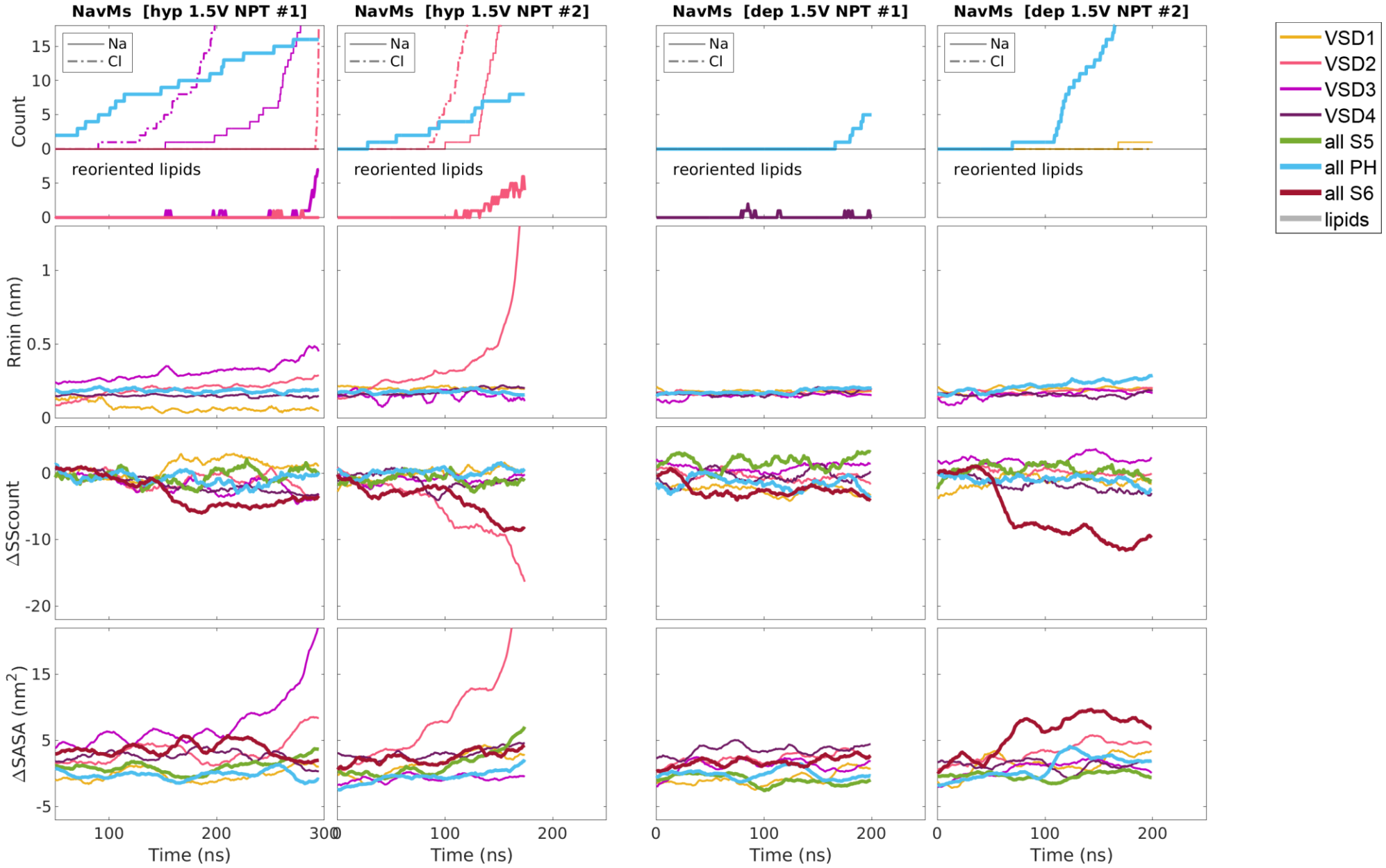

Fig. S10: Additional results for control simulations of NavMs under applied electric field in NPT ensemble.

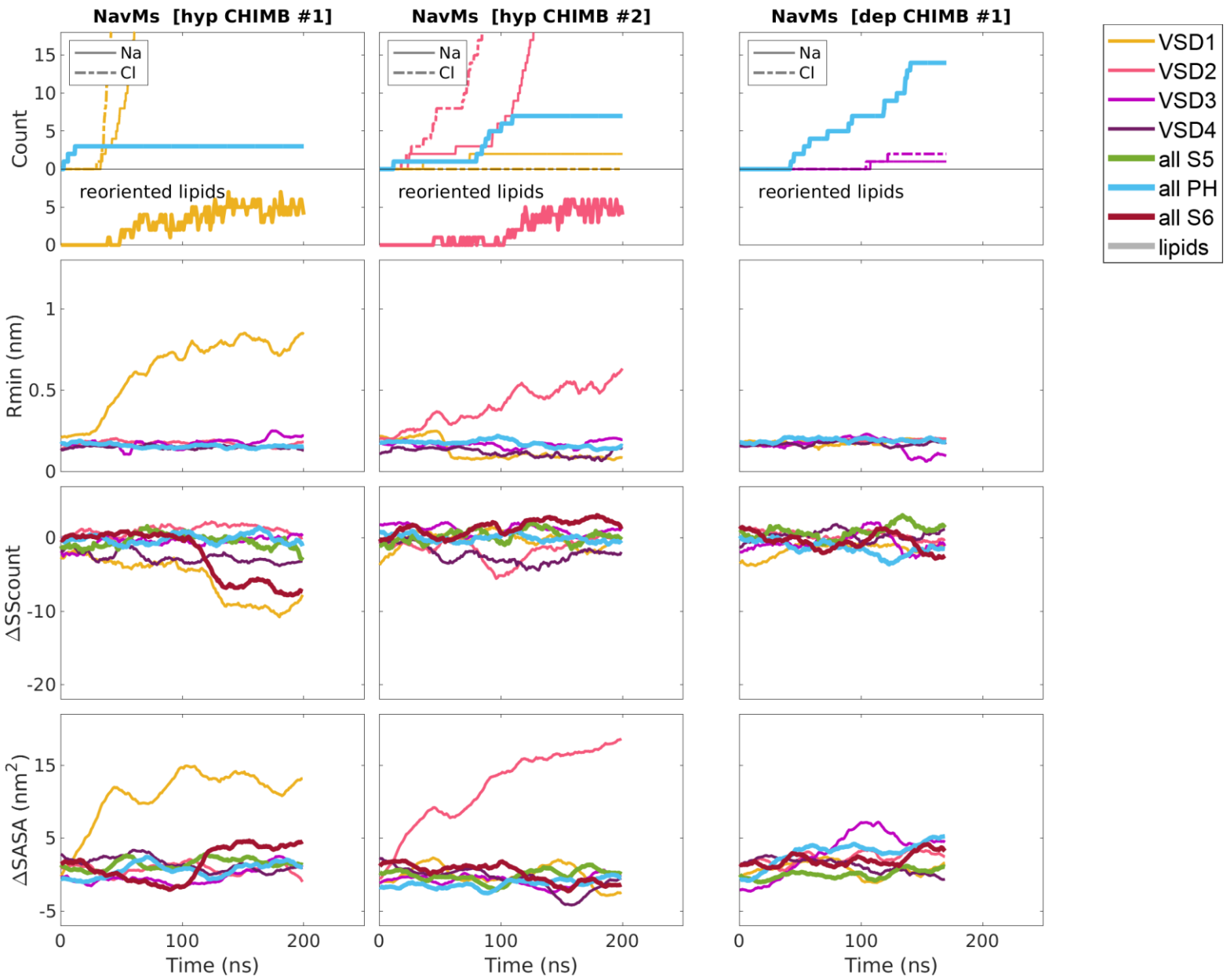

Fig. S11: Additional results for simulations of NavMs under charge imbalance.

S5. VSD hydration

To determine hydration of individual VSDs we used the following approach. We took 200 frames, separated by 1 ns, from the last 200 ns of equilibration. We aligned the frames using MDAnalysis (3, 4) by minimizing the RMSD of the position of Cα atoms in i-th VSD. This yielded 4 aligned trajectories. From the trajectory aligned on i-th VSD we extracted the positions of water oxygen atoms relative to the center of mass i-th VSD. We then plotted these positions into a 2D profile, considering a cylindrical coordinate system (r,z) centered at the VSD's center of mass (see Fig. S12). By looking at these profiles we determined that it is sufficient to consider only the positions of water molecules that are within $r \leq 1.2$ nm and $|z| \leq 1.5$ nm (highlighted with red in Fig. S12). We calculated the kernel-smoothed probability density function (pdf) of the z coordinates with Matlab function ksdensity() using bandwidth of 0.4 Å. The calculated pdf is shown in Fig. S13 together with a histogram of water positions along z coordinate. From the pdf we estimated the free energy F of water molecules as $F = -kT \log(pdf)$. We also tested different bandwidths for calculating the pdf, from 0.2 Å to 1 Å. The conclusions drawn from the free energy estimates, i.e., that pore formation is more likely in VSDs with low free energy barriers for water permeation, were the same for all bandwidths in this range, see Fig. S17. Increasing the bandwidth beyond 1 Å resulted in over-smoothing.

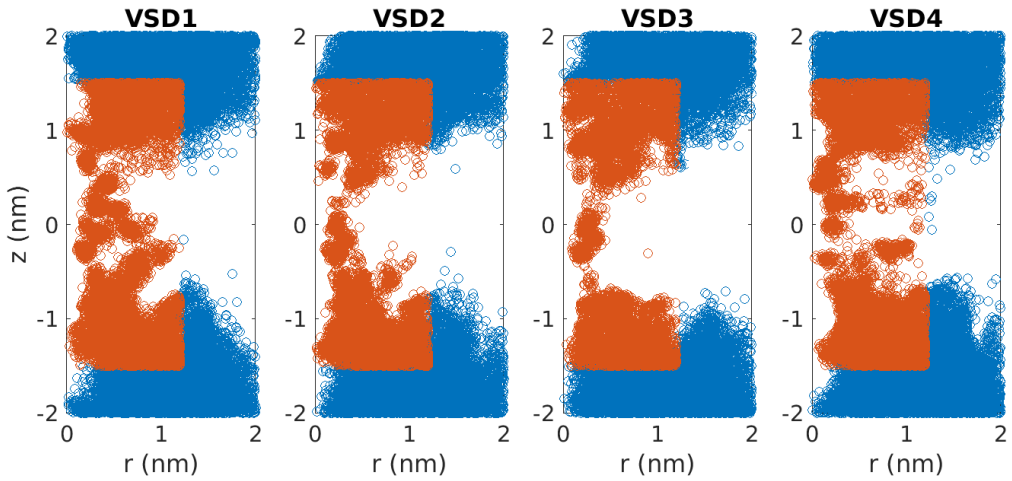

Figure S12: Positions of water molecules in each VSD of NavMs projected along the VSD radius (r) and the VSD principal axis (z). The VSDs' center of mass is located at (0,0). Blue circles show all positions extracted from 200 frames of equilibration trajectory, red circles show the positions that were used in the histograms.

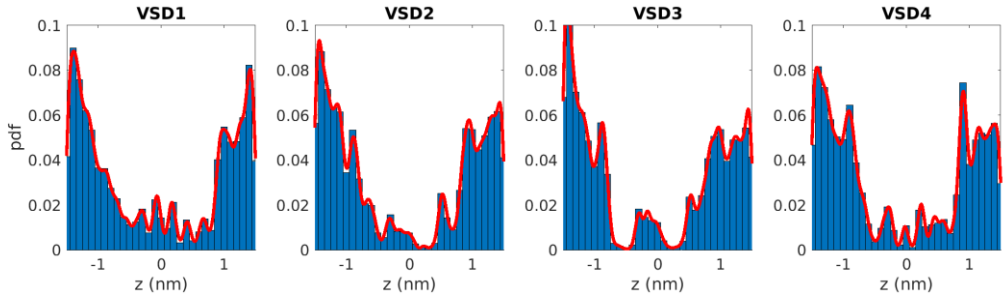

Figure S13: Histograms of the positions of water molecules along z coordinate. Histograms were determined based on positions highlighted with red in Fig. S9. The red lines show the smoothed probability density function.

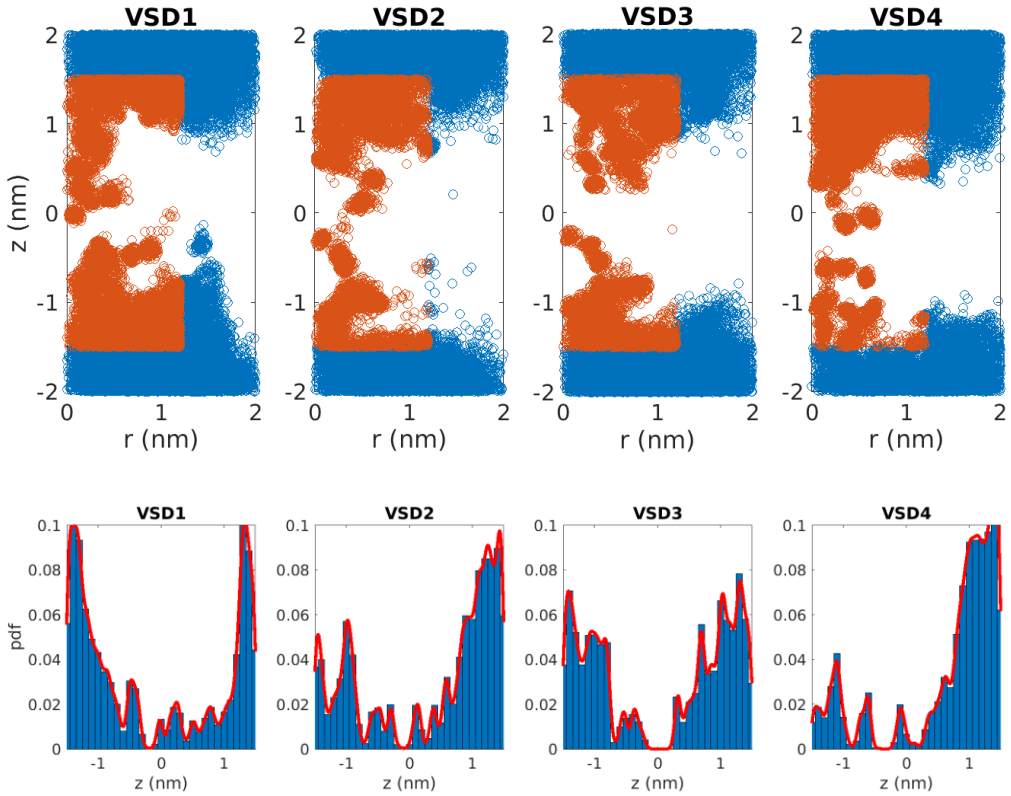

Figure S14: Same as in Fig. S9 and S10, but for NavPaS.

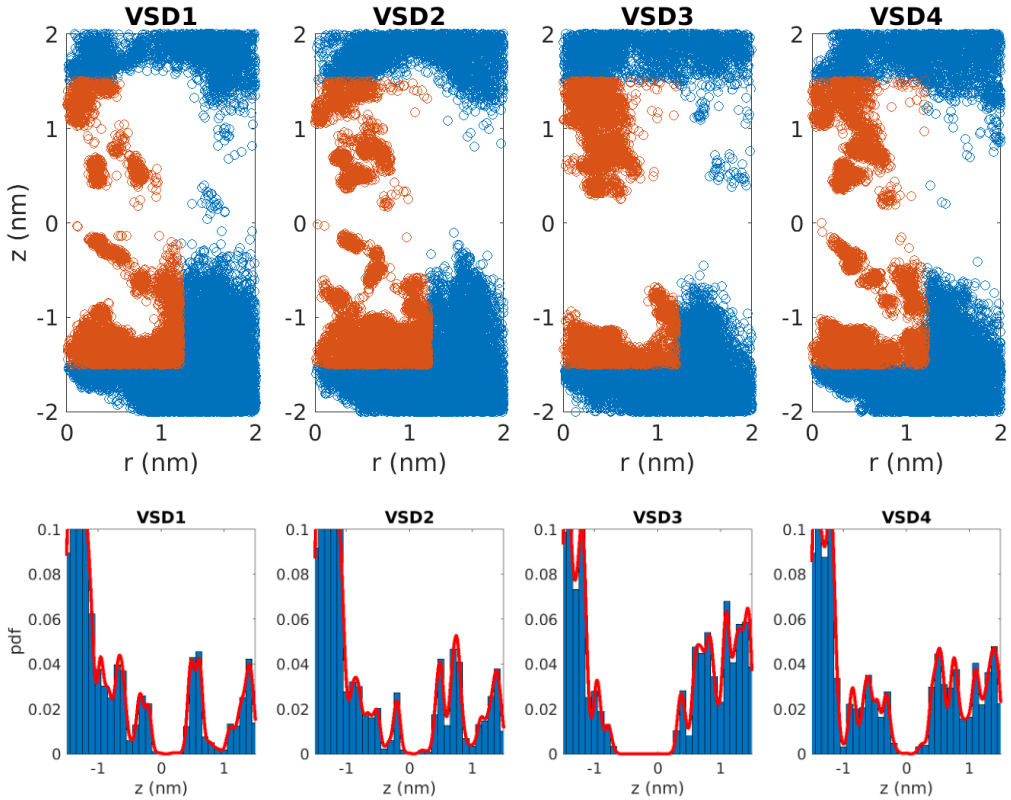

Figure S15: Same as in Fig. S9 and S10, but for wild-type HCN1.

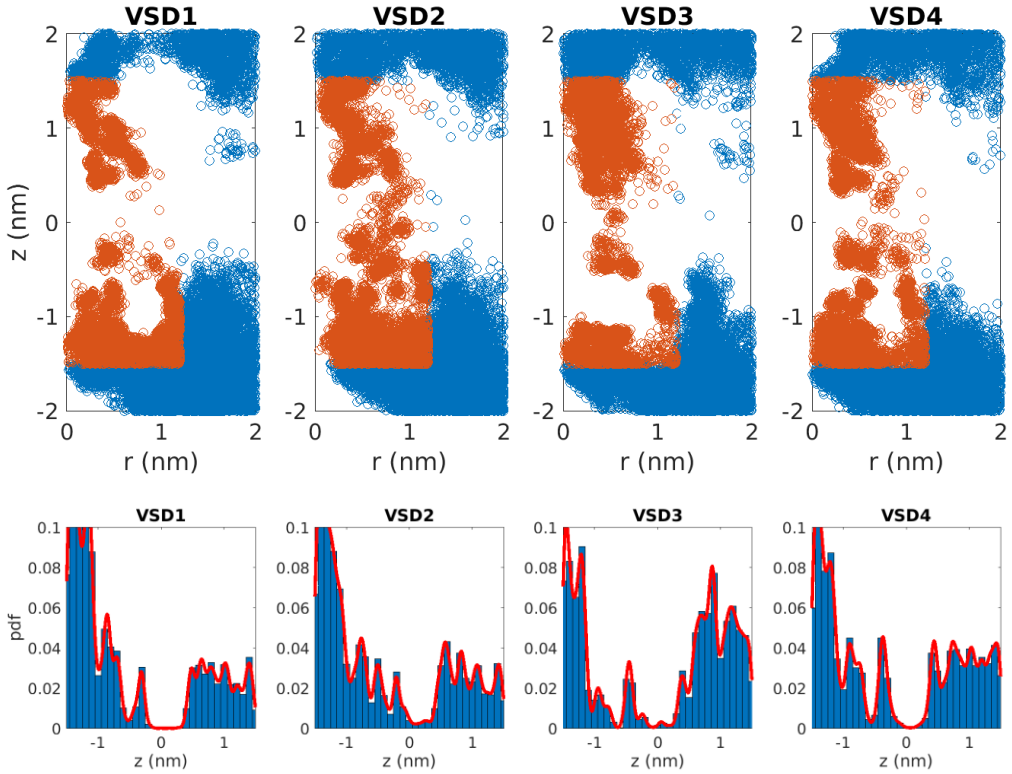

Figure S16: Same as in Fig. S9 and S10, but for mutant HCN1.

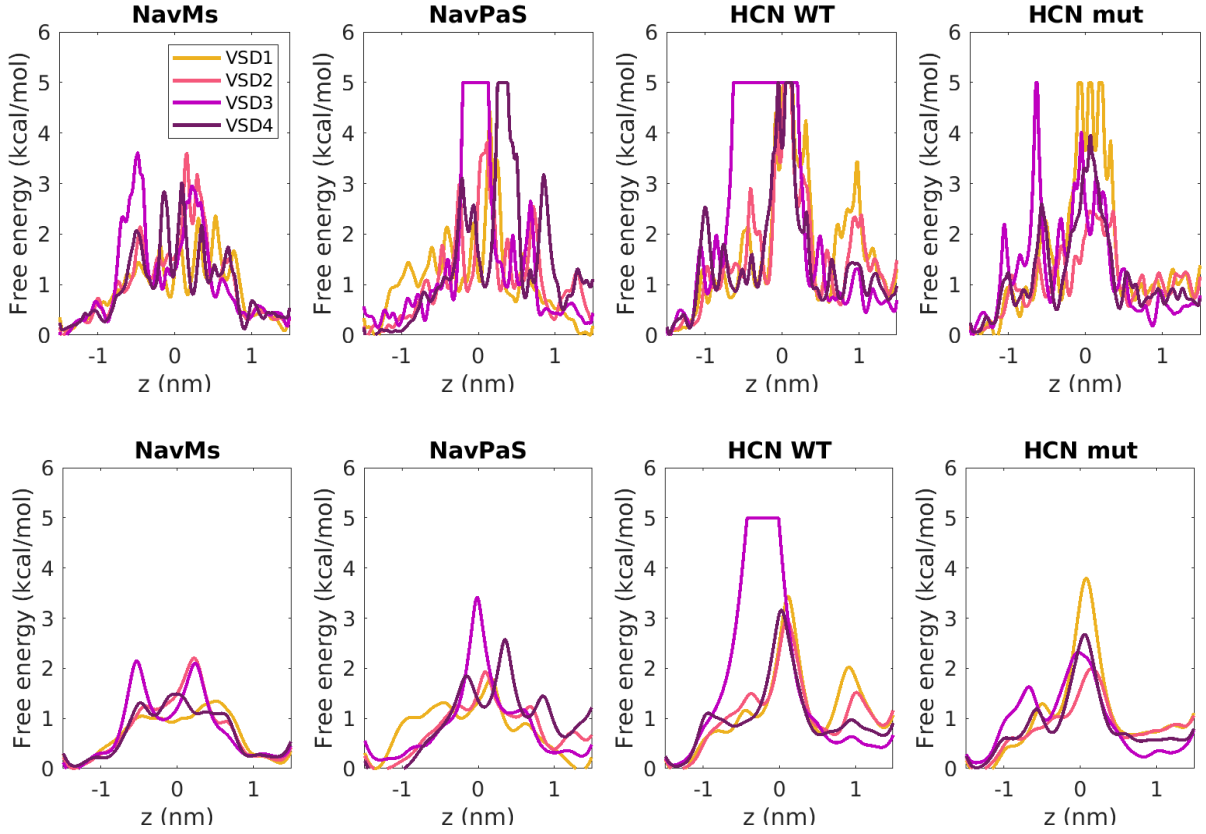

Figure S17: Free energy profiles obtained using bandwidth 0.2 Å (left) and 1 Å (right).

S6. Electrostatic profiles along VSDs

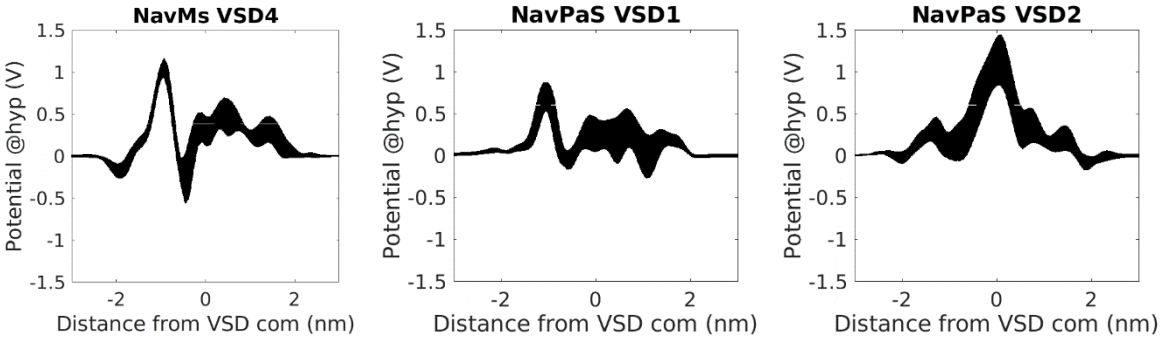

Figure S18: Electrostatic profiles along VSD4 of NavMs, VSD1 of NavPaS, and VSD2 of NavPaS without applied electric field.

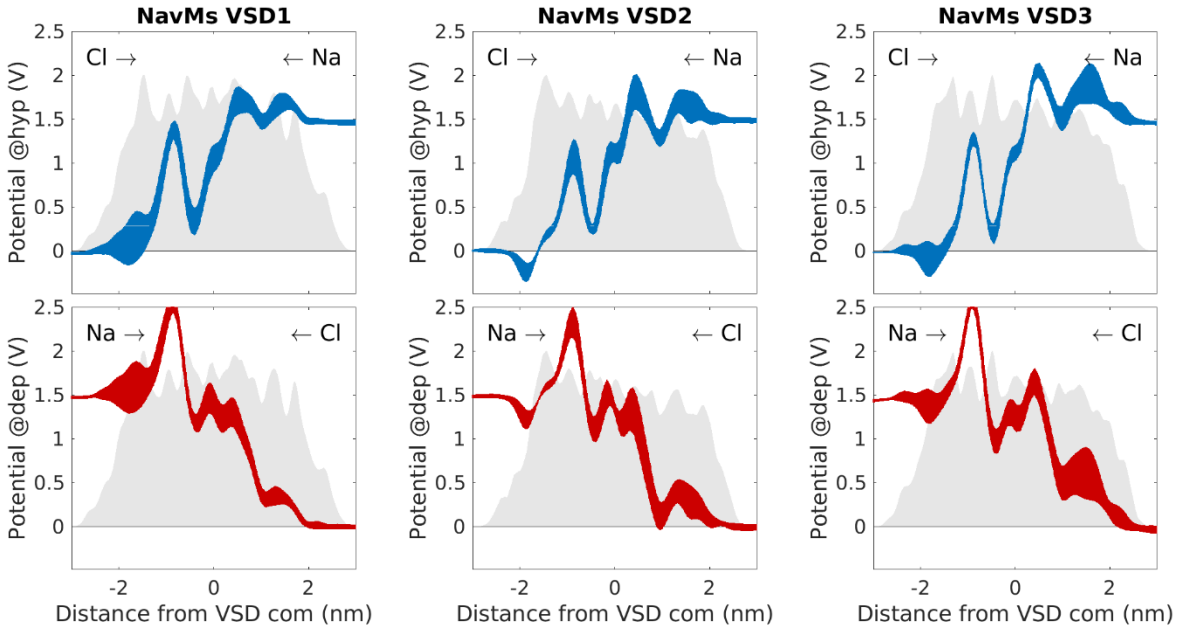

Figure S19: Electrostatic profiles along VSD1, VSD2, and VSD3 of NavMs channel under applied electric field.

S7. Asymmetric conduction through pores in different VSDs

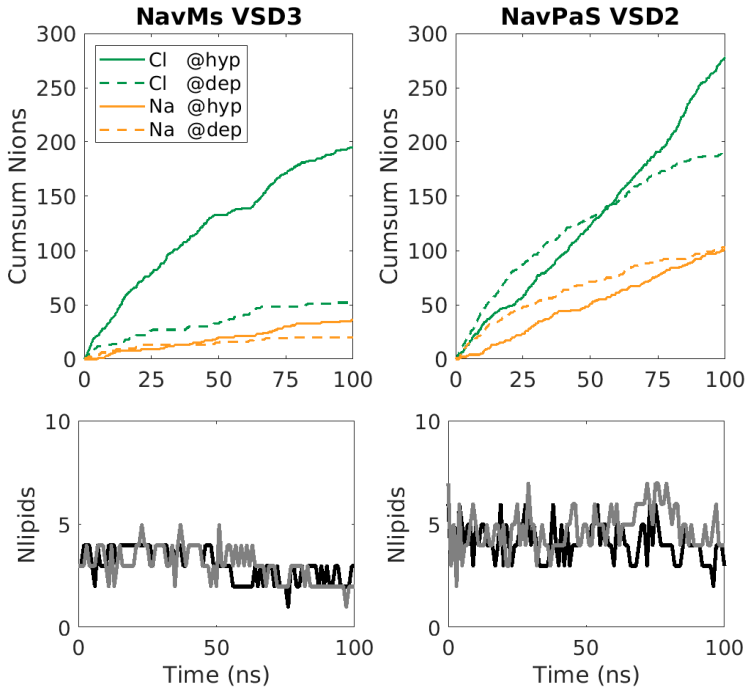

Figure S20: Cumulative sum of the number of ions that passed a complex pore formed in VSD3 of NavMs and VSD2 of NavPaS. Simulations were performed under hyperpolarizing and depolarizing electric fields with 3x lower amplitude (E_z L_z = 0.5 V). The top graphs show that the passage of ions depends on the polarity of TMV in the complex pore of NavMs. The bottom graphs show the number of lipid phosphorus atoms that are close to the VSD pore and within 0.5 nm of the z-position of lipid bilayer's center of mass. The number of lipids that are stabilizing the complex pore does not depend on the TMV polarity.

S8. Complex pores after exposure to electric field

Here we show how the secondary structure of VSDs, in which complex pores formed, remain perturbed after turning off the electric field.

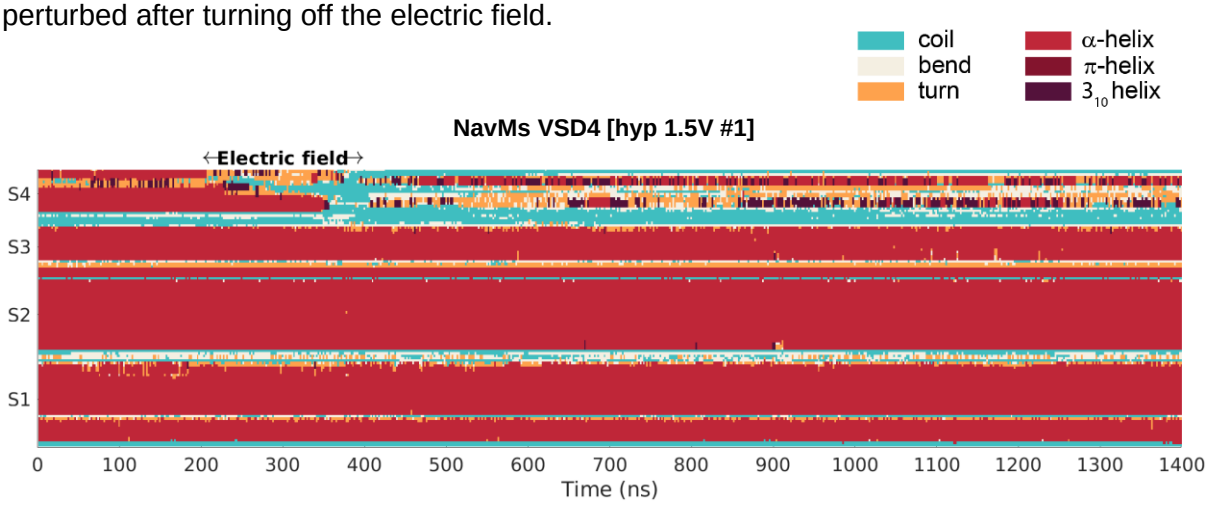

Figure S21: The secondary structure of NavMs VSD4, in which a complex pore was formed in simulation [hyp 1.5V #1], does not recover even 1 μs after turning off the electric field. Electric field was applied t = 200 ns and maintained until t = 400 ns.

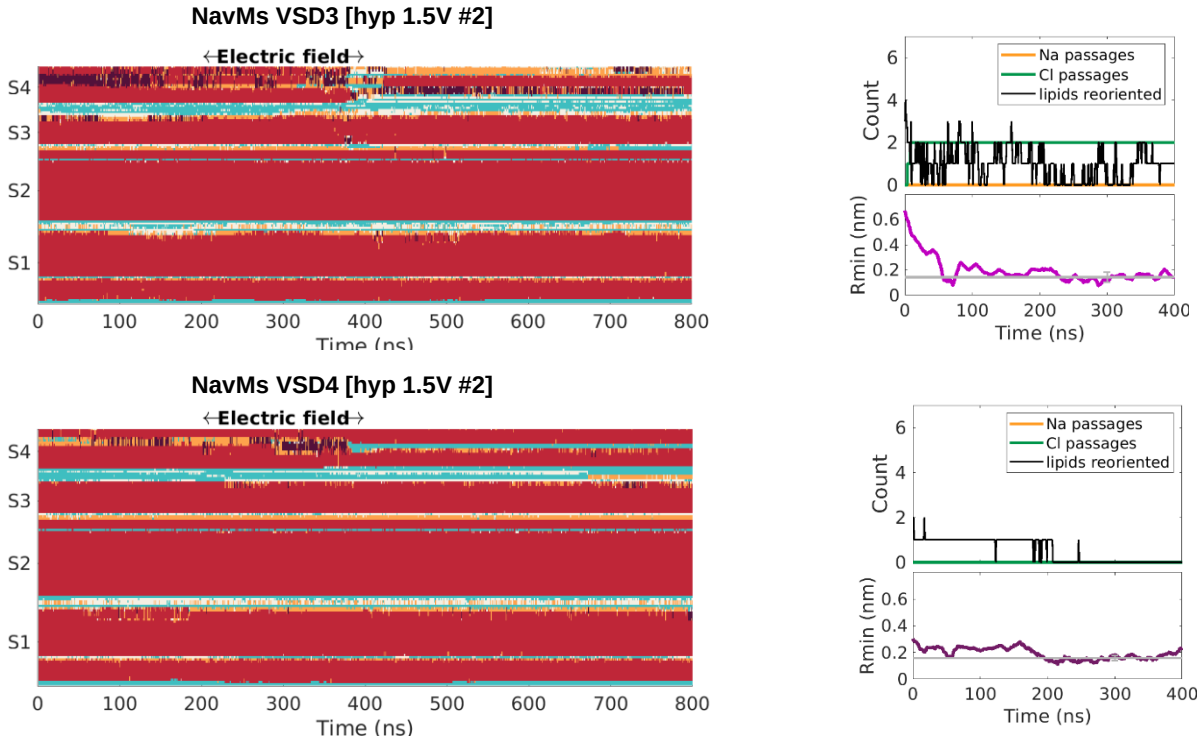

Figure S22: The secondary structure of NavMs VSD3 and VSD4, in which complex pores were formed in simulation [hyp 1.5V #2]. The complex pore in VSD4 barely met the criterion for a complex pore as it became stabilized by two lipids only. Electric field was applied at t = 200 ns and maintained until t = 400 ns. The graphs on the right show the corresponding cumulative sum of Na and Cl ions that passed the pore, the number of lipids that stabilized the pore, and the pore radius after turning off the electric field.

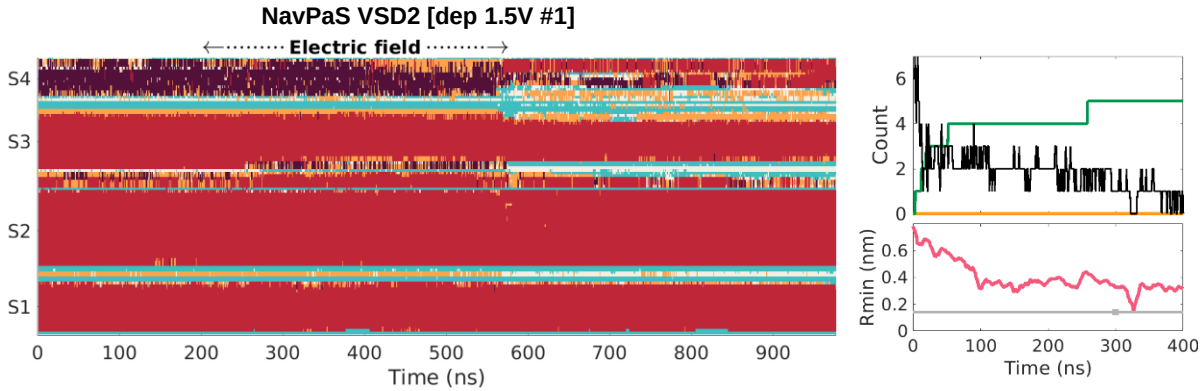

Figure S23: The secondary structure of NavPaS VSD2, in which a complex pore was formed in simulation [dep 1.5V #1]. Electric field was applied t = 200 ns and maintained until t = 576 ns. The graphs on the right show similar as the ones in Fig. S22.

S9. Breakage and formation of salt bridges

An example of how existing salt bridges in VSDs can break and new salt bridges can form is presented for NavMs channel under hyperpolarizing TMV. Figures S24-S27 show the shortest distance between the four arginine residues on S4 (ARG100, ARG103, ARG106, and

ARG109) and acidic residues on S2 and S3. The distances are plotted for the last 200 ns of equilibration (time -200 ns to 0 ns), followed by 200 ns under hyperpolarizing 1.5 V (time 0 ns to 200 ns), and 1 μs after turning off the electric field (time 200 ns to 1200 ns). Note that a VSD pore was formed in VSD1 and VSD4 during an electric field application. A salt bridge is formed when the distance between positive and negative residues decreases to ~0.3 nm.

Tables S4-S5 indicate the salt bridges that were broken and formed in all simulations carried out for each channel.

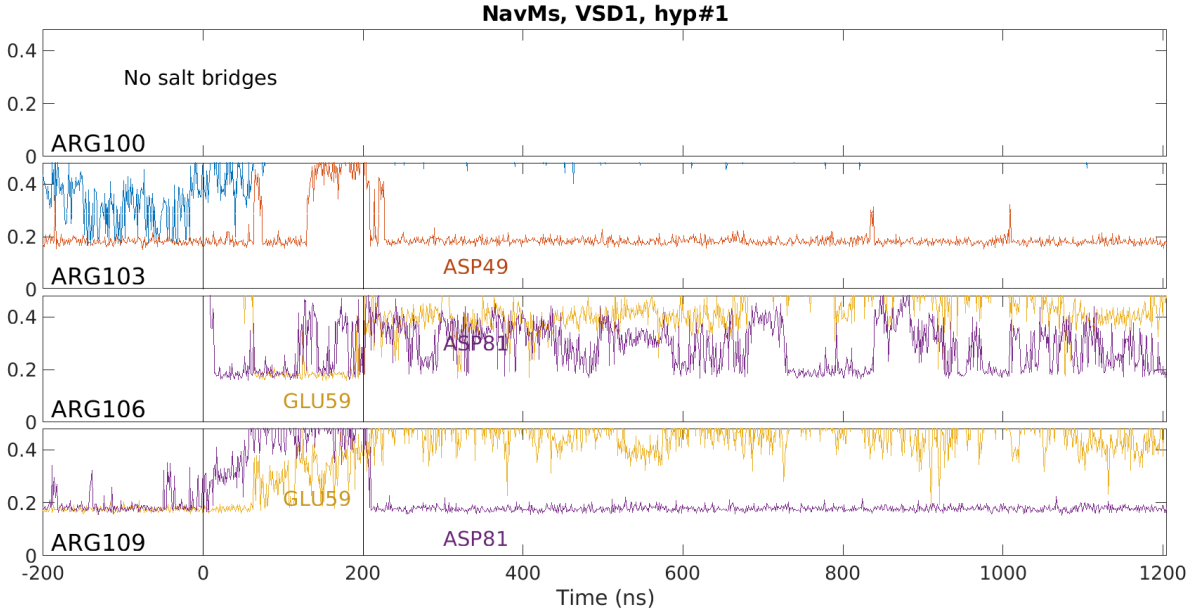

Figure S24: Distances between arginine residues on S4 and acidic residues on S2 and S3 in VSD1. There was a VSD conduit formed in this VSD. All three salt-bridge connections, ARG103-ASP49, ARG109-GLU59, and ARG109-ASP81 break during the pulse and two new connections are formed: ARG106-GLU59 and ARG106-ASP81. Two of the broken connections, ARG103-ASP49 and ARG109-ASP81, reform after the pulse. One of the two new connections, ARG106-ASP81, remains present after the pulse (although in an on/off fashion).

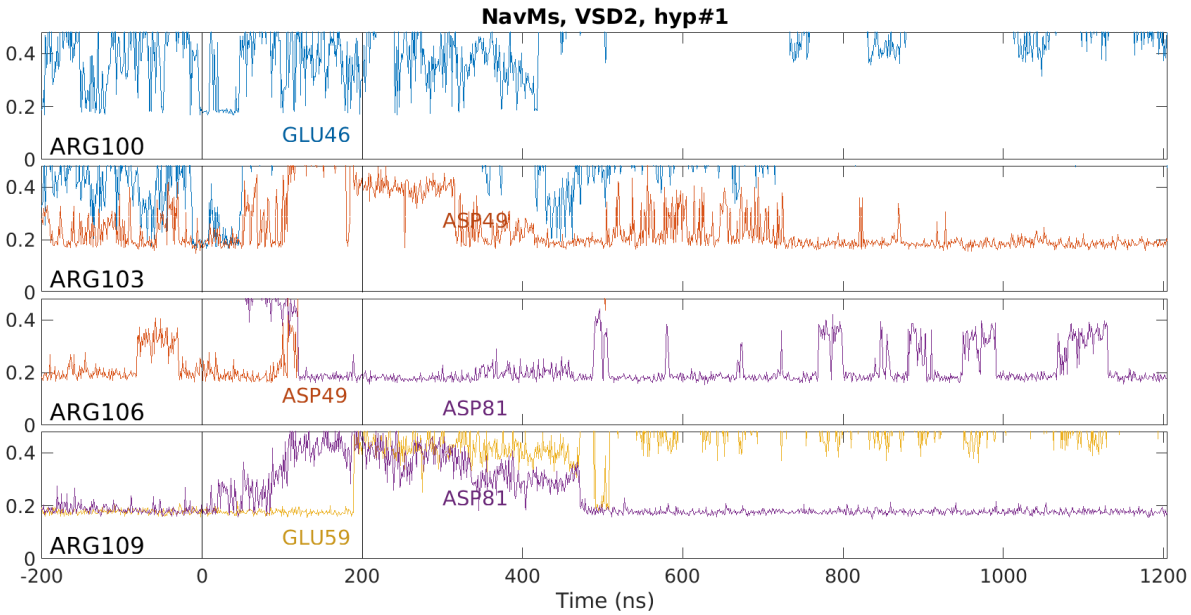

Figure S25: Distances between arginine residues on S4 and acidic residues on S2 and S3 in VSD2. All four salt-bridge connections, ARG103-ASP49, ARG106-ASP49, ARG109-GLU59, and ARG109-ASP81 break during the pulse and one new connection is formed: ARG106-ASP81. Two of the broken connections, ARG103-ASP49 and ARG109-ASP81, reform after the pulse. The new connections, ARG106-ASP81, remains present after the pulse.

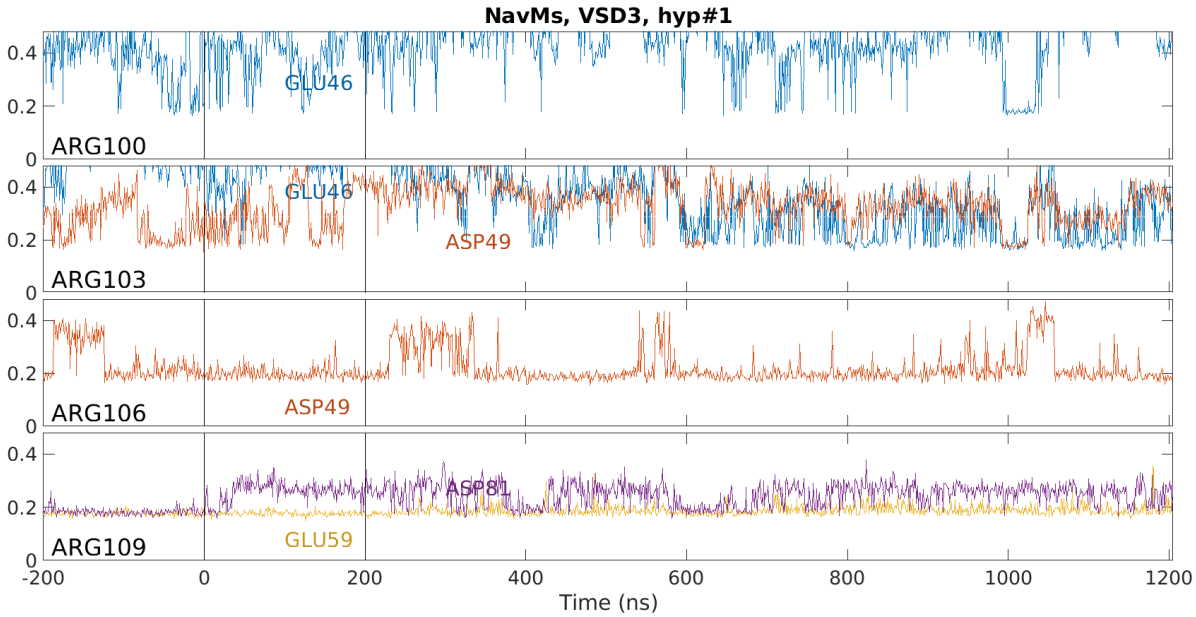

Figure S26: Distances between arginine residues on S4 and acidic residues on S2 and S3 in VSD3. The connection ARG103-ASP49 broke during the pulse and remained broken most of the time after the pulse.

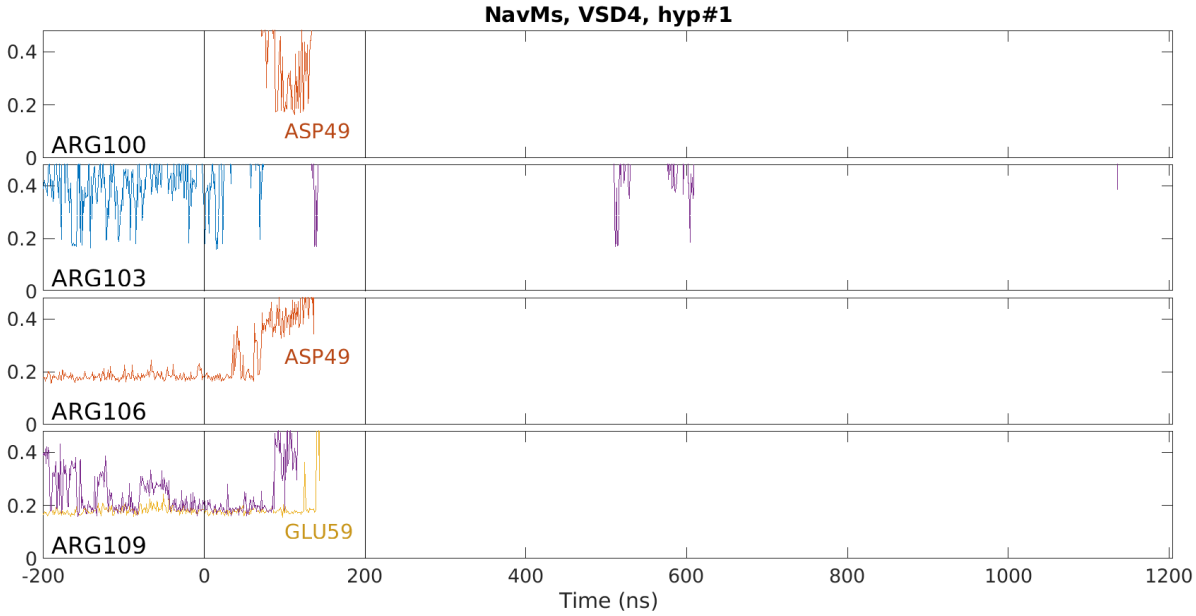

Figure S27: Distances between arginine residues on S4 and acidic residues on S2 and S3 in VSD2. A VSD pore was formed in this VSD. All salt bridge connections break during the pulse and remain broken after the pulse.

Table S6: Salt bridges between positively charged residues on S4 and negatively charged residues on S1-S3 in NavMs. The table lists the initial salt bridges, salt bridges that broke during electric field application (red color) and salt bridges that were formed anew (blue color). Green background indicates that a VSD pore was formed in that VSD and yellow background indicates that a VSD pore expanded into a complex pore. A salt bridge was considered to exist before the pulse, if the distance between the residues, averaged over last 100 ns of equilibration, was shorter than 0.3 nm. A salt bridge was considered as broken, if the distance between two residues, averaged over last 20 ns of the pulse, exceeded 0.3 nm.

NavMs	Before electric field	hyp #1	hyp #2	dep #1	dep#2	hyp #1 – 1000 ns after pulse
VSD1	ARG103-ASP49 ARG109-GLU59 ARG109-ASP81	ARG103-ASP49 ARG109-GLU59 ARG109-ASP81	ARG109-ASP81	ARG103-ASP49 ARG109-GLU59 ARG109-ASP81	ARG109-ASP81	ARG109-GLU59
		ARG106-GLU59 ARG106-ASP81	ARG106-ASP81	-	ARG106-ASP49	ARG106-ASP81
VSD2	ARG103-ASP49 ARG106-ASP49 ARG109-GLU59 ARG109-ASP81	ARG103-ASP49 ARG106-ASP49 ARG109-GLU59 ARG109-ASP81		ARG103-ASP49 ARG109-GLU59 ARG109-ASP81	ARG103-ASP49 ARG106-ASP49 ARG109-GLU59 ARG109-ASP81	ARG106-ASP49 ARG109-GLU59
		ARG106-ASP81	-	-	-	ARG106-ASP81
VSD3	ARG103-ASP49 ARG106-ASP49 ARG109-GLU59 ARG109-ASP81	ARG103-ASP49	ARG103-ASP49 ARG106-ASP49 ARG109-GLU59 ARG109-ASP81	ARG103-ASP49 ARG106-ASP49 ARG109-GLU59 ARG109-ASP81	ARG109-ASP81	ARG103-ASP49
		-	-	-	-	-
VSD4	ARG106-ASP49 ARG109-GLU59 ARG109-ASP81	ARG106-ASP49 ARG109-GLU59 ARG109-ASP81	ARG106-ASP49 ARG109-ASP81	ARG106-ASP49 ARG109-GLU59 ARG109-ASP81	-	ARG106-ASP49 ARG109-GLU59 ARG109-ASP81
		-	-	-	-	-

Table S7: Same as in Table S6, but for NavPaS.

NavPaS	Before electric field	hyp #1	hyp #2	dep #1	dep#2	dep #2 – 400 ns after pulse
VSD1	ARG227-ASP219 ARG233-GLU179 ARG233-ASP205 ARG236-ASP205	ARG236-ASP205	ARG227-ASP219	ARG233-GLU179 ARG233-ASP205 ARG236-ASP205	ARG233-GLU179 ARG233-ASP205 ARG236-ASP205	ARG233-GLU179 ARG233-ASP205 ARG236-ASP205
				-	ARG236-GLU179	ARG236-GLU179
VSD2	ARG613-GLU597 ARG619-GLU565 ARG619-ASP587	ARG613-GLU597 ARG619-GLU565 ARG619-ASP587	ARG613-GLU597 ARG619-GLU565 ARG619-ASP587	ARG613-GLU597 ARG619-GLU565 ARG619-ASP587	ARG613-GLU597 ARG619-GLU565 ARG619-ASP587	ARG613-GLU597 ARG619-GLU565 ARG619-ASP587
		ARG613-ASP587 ARG619-GLU522 LYS622-GLU522		ARG616-GLU597 LYS622-ASP587	-	ARG616-ASP539
VSD3	ARG951-GLU876 ARG951-ASP894 ARG954-GLU876 ARG957-GLU904 ARG957-ASP926	ARG954-GLU876	ARG954-GLU876	ARG951-GLU876 ARG951-ASP894 ARG957-GLU904	-	-
		-		-	-	-
VSD4	HIS1191-ASP1190 ARG1271-ASP1237 ARG1274-GLU1216 ARG1274-ASP1237 ARG1277-ASP1231	ARG1277-ASP1231	ARG1277-ASP1231	-	ARG1277-ASP1231	ARG1277-ASP1231
		-		-	-	-

Table S8: Same as in Table S6, but for wild-type HCN1. Note that the S4 helix in HCN1 is considerably longer than in Nav channels and contains a greater number of charged residues.

HCN1	Before electric field	hyp #1	hyp #2	dep #1
VSD1	ARG252-GLU240, ARG267-ASP183 ARG267-ASP233, ARG270-ASP183 ARG273-ASP189, ARG273-ASP225 ARG276-ASP225, HIS279-GLU282 HIS286-GLU282, HIS286-GLU283	-	ARG273-ASP189 HIS279-GLU282	ARG273-ASP189 HIS279-GLU282
		-	-	-
VSD2	ARG252-GLU240, ARG267-ASP183 ARG267-ASP233, ARG270-ASP183 ARG273-ASP189, ARG273-ASP225 ARG276-ASP225, HIS279-GLU282 HIS286-GLU282, HIS286-GLU283	-	HIS279-GLU282	ARG273-ASP189 HIS279-GLU282
		-	-	-
VSD3	ARG267-ASP183, ARG267-ASP233 ARG270-ASP183, ARG273-ASP189 ARG273-ASP225, ARG276-ASP225 HIS279-GLU282, HIS286-GLU282 HIS286-GLU283	ARG270-ASP183 ARG273-ASP189 ARG276-ASP225 HIS286-GLU282	-	HIS279-GLU282
		-	LYS261-GLU240	-
VSD4	ARG252-GLU240, ARG267-ASP183 ARG267-ASP233, ARG270-ASP183 ARG273-ASP189, ARG273-ASP225 ARG276-ASP225, HIS279-GLU282 HIS286-GLU282, HIS286-GLU283	HIS286-GLU282	ARG267-ASP183 ARG267-ASP233 ARG270-ASP183 ARG273-ASP189 ARG276-ASP225 HIS279-GLU282	-
		-	ARG270-ASP225	ARG252-ASP244

S10. HCN1 mutant under TMV of +0.7 V

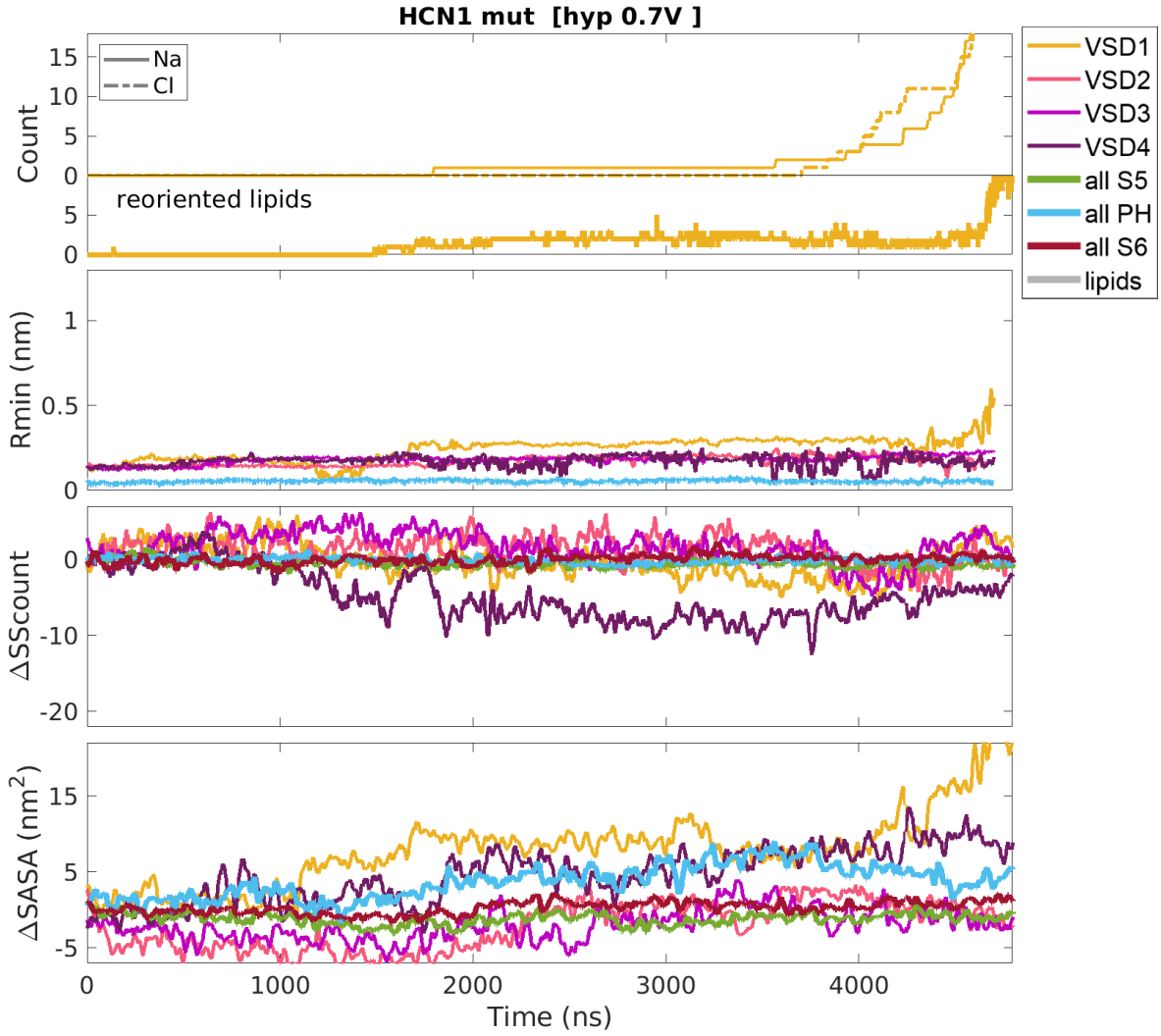

Figure S28: Creation of a complex pore in HCN1 mutant under hyperpolarizing TMV of 0.7 V. The graphs are constructed in the same way as in Fig. S1.